Published in final edited form as:

Cell Rep. 2016 May 3; 15(5): 1100–1110. doi:10.1016/j.celrep.2016.03.087.

Mechanistic Insights into Cofactor-Dependent Coupling of RNA Folding and mRNA Transcription/Translation by a Cobalamin Riboswitch

Jacob T. Polaski[1], **Erik D. Holmstrom**[1,3], **David J. Nesbitt**[1,2], and **Robert T. Batey**[1,*]

[1]Department of Chemistry and Biochemistry, University of Colorado at Boulder, Campus Box 596, Boulder, CO 80309-0596, USA

[2]JILA, University of Colorado and National Institute of Standards and Technology, Campus Box 440, Boulder, CO 80309-0440, USA

SUMMARY

Riboswitches are mRNA elements regulating gene expression in response to direct binding of a metabolite. While these RNAs are increasingly well understood with respect to interactions between receptor domains and their cognate effector molecules, little is known about the specific mechanistic relationship between metabolite binding and gene regulation by the downstream regulatory domain. Using a combination of cell-based, biochemical, and biophysical techniques, we reveal the specific RNA architectural features enabling a cobalamin-dependent hairpin loop docking interaction between receptor and regulatory domains. Furthermore, these data demonstrate that docking kinetics dictate a regulatory response involving the coupling of translation initiation to general mechanisms that control mRNA abundance. These results yield a comprehensive picture of how RNA structure in the riboswitch regulatory domain enables kinetically constrained ligand-dependent regulation of gene expression.

In Brief

Polaski et al. reveal specific structural features of cobalamin riboswitches that couple ligand binding to regulation of gene expression. Unusual structural features within a kissing loop interaction, coupled with the kinetics of its assembly, produce a regulatory response that controls both ribosome loading and mRNA abundance.

*Correspondence: robert.batey@colorado.edu.

[3]Present address: Department of Biochemistry, University of Zurich, Winterthurerstrasse 190, 8057 Zurich, Switzerland

AUTHOR CONTRIBUTIONS

J.T.P. performed all biochemical and cell-based experiments, and E.D.H. performed all single-molecule experiments. All authors interpreted data and assisted with the manuscript preparation. J.T.P. and R.T.B. wrote the manuscript.

SUPPLEMENTAL INFORMATION

Supplemental information includes Supplemental Experimental Procedures, seven figures, and two tables and can be found with this article online at http://dx.doi.org/10.1016/j.celrep.2016.03.087.

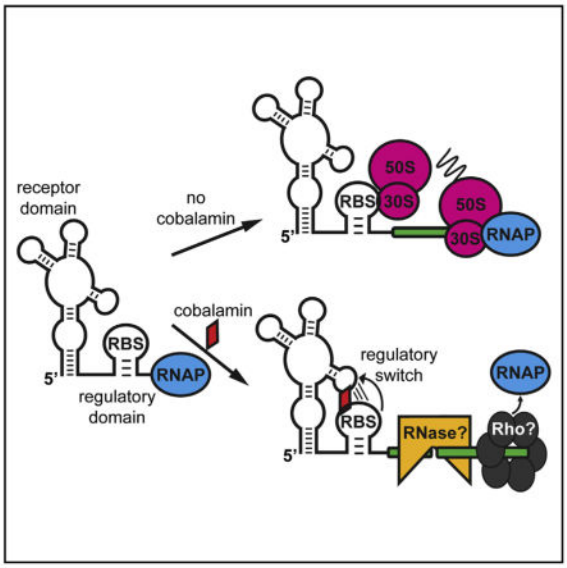

INTRODUCTION

Bacterial RNA-based genetic regulatory mechanisms are critical for maintenance of normal cellular homeostasis and response to a spectrum of environmental and intracellular signals (Roth and Breaker, 2009; Storz et al., 2011). Riboswitches represent one of the most parsimonious solutions to regulating gene expression in response to intracellular metabolites and other signals (Roth and Breaker, 2009). Typically, riboswitches are found in the leader regions of bacterial mRNAs and function through the interplay between two domains: a highly structured receptor (aptamer) domain that directly binds a small molecule effector and a downstream regulatory domain (expression platform) containing a structural switch that instructs the expression machinery. Over the last decade, the receptor domains of riboswitches have become important model systems for understanding many questions related to RNA biology and chemistry, including folding, basic principles of RNA structure, design of small molecules targeting RNAs, and design of novel RNA-based biosensors for interrogating cellular processes (Porter et al., 2014). Despite these advances, little is known about how the occupancy status of the receptor dictates the structural fate of the downstream switch responsible for modulating gene expression for most riboswitches.

Recently, the crystal structure of a cobalamin-binding riboswitch containing discrete receptor and regulatory domains was determined (Johnson et al., 2012). As the only riboswitch structure experimentally demonstrated to comprise all sequence elements necessary and sufficient for ligand-dependent gene regulation in a biological context, this presents a unique opportunity to understand how effector binding and regulatory activity are mechanistically coupled. Cobalamin (vitamin B_{12})-binding riboswitches are the second-most-widely distributed riboswitch in biology (Barrick and Breaker, 2007), generally regulating biosynthesis or transport of this important cofactor (Nahvi et al., 2002; Vitreschak et al., 2003). This structure revealed that the central four-way junction of the receptor domain contacts the variable R-group and β-axial face of the corrin ring of cobalamin, while

the α-axial face of the ligand directly contacts an interdomain kissing loop (KL) interaction formed between the loops of hairpins P5 of the receptor and P13 of the regulatory domain (Figures 1A and 1B; Johnson et al., 2012). Chemical probing of the RNA reveals that under physiological magnesium ion concentrations, the KL interaction is strictly cobalamin dependent, and ablation of this interaction abolishes ligand-dependent gene regulation. Subsequent work using single-molecule fluorescence resonance energy transfer (smFRET) determined that cobalamin significantly increases the lifetime of the KL in the docked conformation (Holmstrom et al., 2014), further establishing the direct link between ligand binding and the structural switch.

The KL motif has been found to mediate a spectrum of biological processes, including retroviral RNA dimerization for packaging, regulation of plasmid replication, and establishment of higher-order RNA architecture (Butcher and Pyle, 2011). This RNA module is formed through Watson-Crick base pairing of two terminal hairpin loops to form a third helix that stacks between the helical stems of the two hairpins. In almost all known examples that have been studied, base-pairing interactions throughout the entirety of the interloop helix allow this module to self-assemble. Therefore, it was unexpected to find that gene regulation by the cobalamin riboswitch relies on a cobalamin-dependent structural change based on KL formation.

As a model system, we studied a member (*env8*HyCbl; GenBank: AACY021350931.1) of the 5′-deoxyadenosylcobalamin (AdoCbl)-variant family (Rfam: RF01689) that preferentially interacts with cobalamin derivatives possessing small β-axial ligands such as hydroxocobalamin (HyCbl) or methylcobalamin while discriminating against larger analogs like AdoCbl (Johnson et al., 2012). Using a combination of cell-based, biochemical, and biophysical experiments, two key structural features of the cobalamin riboswitch expression platform were found to be important for conferring ligand-dependent genetic regulation. First, unpaired nucleotides within the regulatory KL destabilize this module and confer cobalamin dependency to the structural switch (Figures 1C and 1D). Second, while this interaction can occur in *trans* in vitro, we find it is highly context dependent in an mRNA, where the proximity between receptor and regulatory domains (which is determined by the length of a single-stranded joining region) has a strong influence on efficient regulation. Although cobalamin-dependent formation of the KL occludes the ribosome-binding site (RBS) in the regulatory domain hairpin, thereby directly repressing translation, other mechanisms controlling mRNA abundance play important roles in eliciting the full regulatory response.

RESULTS

Unusual Structural Features in the Interdomain KL Are Essential for Cobalamin-Dependent Gene Regulation

The regulatory KL of cobalamin riboswitches has conserved non-canonical base pairs, as well as unpaired nucleotides interrupting the helix formed by base pairing of the loops of helices 5 and 13 (L5 and L13), a feature not observed in other biological representatives of this motif. In the *env8*HyCbl structure two unpaired purines (A97 and G98) are observed between the A48•G96 and the U45-A99 pairs (Figures 1C and 1D). Alignment of 144

sequences in the AdoCbl-variant family reveals that both the position and the number of unpaired nucleotides is strictly conserved (Table S1). The uniqueness of bulged nucleotides and/or non-Watson-Crick base pairs in the KL between the domains suggests these structural features may be central to the mechanism of cobalamin-dependent gene regulation.

To determine the relationship between non-canonical features in the KL and regulatory activity, we used an *E. coli*-based reporter system that places expression of a fluorescent protein reporter (GFPuv) under control of the *env8*HyCbl riboswitch. This assay was previously demonstrated to report on *env8*HyCbl regulatory activity in a cobalamin- and KL-dependent fashion (Johnson et al., 2012). Cells expressing the reporter under control of the wild-type (WT) riboswitch exhibit ~8.5-fold repression of fluorescence when grown in the presence of 5 μM HyCbl compared to cells grown in the absence of ligand (Figure 2; Figure S1). Consistent with the KL mediating the cobalamin-dependent regulatory response, activity is lost when the L5 sequence is changed to a 5′-GAAA-3′ tetraloop (variant *ko*) that cannot base pair with L13.

The role of the non-Watson-Crick base pair was interrogated by introducing a series of systematic mutations into L5 that either stabilize or destabilize the interaction. Mutations were introduced only into L5 as to not disrupt the ability of the ribosome to recognize the RBS in L13. Regulatory activity was ablated when nucleotides were inserted into L5 to pair with the bulged nucleotides in L13 while retaining the non-canonical A•G base pair (variants *a*–*c*; Figure 2). Cells expressing these mutants show variable levels of gene expression when grown in both the absence and the presence of ligand, suggesting not all insertions have a stabilizing effect on KL formation in the context of the A•G base pair (variants *a*–*c*; Figure S1). In contrast, riboswitches harboring a 46A_C substitution in L5 that converts the non-canonical A•G pair to a G-C Watson-Crick base pair regulate gene expression at levels comparable to the WT RNA (variant *d*; Figure 2), consistent with this pair varying between Watson-Crick and purine-purine non-canonical pairs in phylogeny (Table S1). Cells expressing mutant RNAs containing insertions in L5, in addition to the 46A_C substitution, also possess regulatory function, albeit with a dynamic range lower than that of the WT riboswitch (variants *e* and *f*; Figure 2). The decline in dynamic range can be attributed mostly to decreased fluorescence in the absence of ligand, because cells expressing these mutants repress gene expression to similar levels as the WT riboswitch when grown in the presence of saturating HyCbl (variants *d*–*f*; Figure S1). Regulatory activity was lost, however, when nucleotides were inserted into L5 that promote Watson-Crick base pairing throughout the entirety of the KL (variant *g*; Figure 2). Cells expressing this mutant riboswitch exhibit levels of fluorescence near background when grown in both the presence and the absence of ligand, suggesting perfect base pairing promotes HyCbl-independent KL assembly (variant *g*; Figure S1).

The KL interaction is intolerant of changes that further destabilize the tertiary interaction. Deletion of a single nucleotide in L5 on either side of the bulged purines in L13 results in a nonfunctional riboswitch (variants *h* and *i*; Figure 2). Specifically, eliminating the A•G base pair by deletion of A46 or eliminating the U-A Watson-Crick pair by deletion of U45 diminished regulatory activity to levels comparable to the L5(5′-UGAAAG-3′) mutant. However, unlike the insertions in L5 described earlier, cells expressing both deletion mutants

showed high levels of reporter expression in the absence and presence of ligand, suggesting these mutations constitutively destabilize KL formation even in the presence of saturating HyCbl (variants *h* and *i*; Figure S1). To validate that the observed changes in regulatory function are not due to impaired ligand binding, six of the ten L5 mutants (at least one sequence for each type of mutation: "bulge repair," "mismatch/bulge repair," or "destabilized KL") were tested by isothermal titration calorimetry (ITC), and none showed a significant decrease in binding affinity (Figure S2). Together, these data establish that in the presence of a non-canonical purine-purine base pair, two bulged purines in the KL are necessary for regulatory activity. However, when the purine-purine base pair is converted to a canonical Watson-Crick base pair, at least one bulged nucleotide on the 3′ side of the KL helix is sufficient for regulation. This result is reflected in the observed variation of the KL module in the more prevalent AdoCbl family (~90% of total sequences in the cobalamin clan, Rfam CL0101), where the size and placement of unpaired nucleotides are variable but at least one unpaired nucleotide is always present.

In addition, we observe that the sequence of L13 must be presented to L5 in the context of a stem loop (SL; Figure S3). This contrasts with the *S*-adenosylmethionine-I/IV (Trausch et al., 2014), cyclic-di-AMP (Gao and Serganov, 2014; Jones and Ferré-D'Amaré, 2014; Ren and Patel, 2014), and class III pre-queuosine$_1$ (preQ$_1$) riboswitches (Liberman et al., 2015), where a pseudoknot motif forms using an unstructured single-stranded sequence 3′ to the receptor domain to mediate the ligand-dependent regulatory response. Like the 5-aminoimidazole-4-carboxamide ribonucleotide (ZMP) riboswitch (Jones and Ferré-D'Amaré, 2015; Ren et al., 2015; Trausch et al., 2015), the requirement for a SL may be due to the direct interactions between ligand and terminal pseudoknot, a feature absent from the other riboswitches.

Cobalamin Directly Stabilizes an Inherently Unstable KL Interaction

To further define the role of cobalamin in stabilizing the KL interaction, a *trans* RNA-RNA interaction assay was employed. Binding of a ^{32}P-labeled SL corresponding to nucleotides 89–102 of the regulatory domain to the receptor domain of the WT riboswitch (nucleotides 1–81) was assessed using an electrophoretic mobility shift assay (EMSA). The isolated receptor domain retains nearly the same affinity for HyCbl as the full-length riboswitch, as determined by ITC, enabling the EMSA to monitor KL formation in the presence and absence of HyCbl (Figures S4A and S4B). Comparison of the WT aptamer and several KL variants in the presence and absence of ligand reveals clear variations in the behavior of the loop-loop interaction, consistent with activity assays (Figures S4C and S4D). As expected, the L5(5′-UGAAAG-3′) mutant receptor domain is unable to shift SL13 in the absence or presence of HyCbl (variant *ko*; Figure 3A), while the 45_46insCU, 46A_C mutant promotes the interaction regardless of the presence of ligand (variant *g*; Figure 3A). In addition, the WT aptamer only interacts with SL13 in the presence of HyCbl (*wt*; Figure 3A). In the absence of HyCbl, receptor domain concentrations exceeding 150 μM are unable to shift SL13, indicating a minimum apparent equilibrium dissociation constant (K_D) of 2 mM. In the presence of HyCbl, the two RNAs have a K_D of 290 nM, corresponding to a >6,800-fold increase in affinity. This contrasts with the 45_46insCU, 46A_C (*g*) mutant that exhibits nearly identical affinities for the KL interaction in both the presence and the absence of

ligand, which correlates with observed low levels of cellular fluorescence and an inability to regulate gene expression in the reporter-based activity assay. Like the 45_46insCU, 46A_C (*g*) variant, the 46A_C aptamer supports SL13 binding in the absence of cobalamin and exhibits 27-fold weaker affinity compared to receptor domain-SL13 binding in the presence of ligand (variant *d*; Figure 3B). Yet despite its ability to promote KL formation in the absence of HyCbl, this RNA regulates gene expression nearly as well as the WT riboswitch, with ~8-fold repression in the reporter assay.

Although the preceding results suggest that large differences in affinity observed in *trans* between the two domains in the absence and presence of cobalamin are generally predictive of an efficient switch in a cellular context, two mutants significantly deviate from this trend. The 45_46insC, 46A_C mutant exhibits 56-fold weaker affinity between the aptamer and SL13 in the absence of cobalamin compared to its presence but shows only ~2-fold repression of cellular fluorescence in the reporter assay (variant *f*; Figure 3C). In contrast, the 45_46insU, 46A_C mutant aptamer shows only 2.4-fold difference in affinity for SL13 in the absence and presence of cobalamin, yet unlike the A45_46insC, 46A_C (*g*) mutant, this sequence supports robust regulatory activity in the reporter assay, exhibiting ~5-fold repression of fluorescence when expressed in cells grown in the presence of cobalamin (variant *e*; Figure 3C). Together, these results demonstrate only a moderate correlation between changes in ligand-dependent KL affinity and regulatory function. This likely reflects a more complex interplay of constraints in the intracellular environment than solely interdomain affinity. For example, different timescales for folding of RNA structure (e.g., kinetics) represent one possible explanation for why some mutants can have cobalamin-facilitated KL formation by EMSA but fail to effectively regulate gene expression in the reporter assay.

Regulatory Activity Is Modulated by a Single-Stranded RNA Sequence that Tethers the Receptor Domain to the Regulatory Domain

Apart from SL13, the other major component of the expression platform is a single-stranded sequence between helices P1 and P13 (J1/13; Figure 1A). Single-stranded joining sequences within structured RNAs are rarely considered to substantially influence biological activity. However, the preceding experiments suggest that both the thermodynamics (binding affinity) and the kinetics (folding timescales) of KL assembly are important for gene regulation, both of which could be heavily influenced by the interdomain linker. If this is the case, the nature of the single-stranded region would affect folding and association kinetics and thus substantially influence regulatory activity. To address this, we constructed mutant riboswitches that feature linkers designed to test the effects of sequence composition, rigidity, and propensity to adopt secondary structure on gene regulation in a cellular context.

The J1/13 linker is highly permissive of sequence variation, but it is intolerant of guanosine. The homopolymeric sequences poly(A), poly(C), and poly(U), as well as linkers exclusively composed of these nucleotides, all display cobalamin-dependent activities. The most active variants are those that are almost exclusively poly(A) or poly(C), with the exception of poly(U) (Figure 4). Variation in the levels of cobalamin-dependent regulatory activity is almost entirely the result of differences in reporter expression levels at low intracellular

cobalamin concentrations. Levels of reporter gene expression in cells grown in the presence of HyCbl expressing J1/13 sequence variants were comparable to those of the WT riboswitch, indicating ligand-dependent KL formation is tolerant of variation in the sequence composition of J1/13 (Figure S5). In contrast, large observed differences of cellular fluorescence from cells grown in the absence of HyCbl suggest the sequence composition of J1/13 modulates the degree of accessibility of the RBS in L13. The relative trend of expression by the riboswitches with homopolymeric linker sequences in the absence of ligand (Figure S5B) is in general agreement with observations of the structure of homo-polymeic single-stranded RNA. While poly(C) and poly(A) are observed to exhibit significant base stacking, poly(U) behaves like a random coil (Seol et al., 2007), enabling L5–L13 docking on a faster timescale. Another hypothesis that may further explain the observed trend is that G-rich sequences may promote misfolding of the transcript, particularly SL13, which would render the message constitutively unable to interact with the translation machinery.

Regulatory Activity Varies as a Function of the Distance Separating the Receptor and Regulatory Domains

To address the effect of spatial proximity between the two domains on cobalamin-dependent regulation, the activity of the riboswitch was measured as a function J1/13 linker length. Systematic additions or deletions were made to the WT linker sequence that extend or shorten its length, and regulatory activity was assessed using the cell-based reporter assay. To determine whether these mutations induce alternative secondary structure formation or disrupt ligand binding to the receptor domain, the structure of a subset of linker mutants was probed in vitro using *N*-methylisatoic anhydride (NMIA) by selective 2′-hydroxyl acylation and primer extension (SHAPE; Merino et al., 2005). The WT linker and all length variants are highly reactive to NMIA in the absence and presence of cobalamin, revealing this region of the RNA is highly conformationally dynamic (Figures 5A and 5B). Like the WT riboswitch, mutants with shorter and longer linkers show decreased NMIA reactivity within the four-way junction of the aptamer in the presence of HyCbl, indicating the mutagenesis strategy does not impair ligand binding. However, only the WT riboswitch shows decreased NMIA reactivity in both L5 and L13 in the presence of ligand, which is diagnostic of ligand-dependent KL formation (Figure 5C). This result suggests the length of the linker sequence influences the efficiency of KL formation.

Analysis of variants spanning linker lengths of 0–45 nucleotides using the cell-based reporter assay revealed a strong spatial relationship between the two domains (Figure S6A). For length variations from 0 to 4 nucleotides, there is no cobalamin-dependent regulation due to a lack of reporter expression in the absence of cobalamin, which could result from steric occlusion of the RBS in SL13 by positioning it proximal to the receptor domain. Further extension of J1/13 from 5 to 19 nucleotides shows a trend of increasing ligand-dependent gene repression, reflecting increasing levels of reporter expression at low cobalamin concentrations (Figure 5D; Figure S6A). In the absence of cobalamin, there is a nearly linear relationship between reporter expression levels and linker lengths spanning 5 to 21 nucleotides (Figure S6B). Further extension of the linker to lengths between 21 and 25 nucleotides continues to support cobalamin-dependent regulation that is at least as strong as

the WT riboswitch. Thus, in this length regime of J1/13, the amplitude of the regulatory response is likely dictated by a higher frequency of ribosome loading onto the mRNA as the two domains are increasingly spatially separated. Another important observation is that the mutant with a 25-nucleotide linker shows a high degree of regulatory activity in the cell-based reporter system, whereas SHAPE probing indicates this variant is unable to form the KL interaction in the presence of ligand. These observations, which are similar to reported differences between SHAPE reactivity profiles and smFRET measurements of docking by the class III preQ$_1$ riboswitch (Liberman et al., 2015), most likely reflect the dynamics of RNA conformational transitions even in the presence of ligand and the long timescales of NMIA probing ~2 hr.

As the linker length is extended beyond 27 nucleotides, cobalamin-dependent regulation is increasingly diminished. In this regime, it appears that multiple factors act upon the riboswitch to diminish regulatory activity. Under low cobalamin concentrations, expression of the reporter is quite variable—systematically lower than the maximal expression levels observed but at least at the level of, or in some cases significantly higher than, the WT sequence (Figure S6A). At saturating concentrations of cobalamin, expression of the reporter is significantly higher compared to riboswitches with linkers of 27 nucleotides and shorter, such that beyond 30 nucleotides the average level of cellular fluorescence is about that of cells expressing the WT RNA in the absence of cobalamin. Together, these results demonstrate a strong proximity effect on regulatory activity and support the hypothesis that the rate of KL assembly acts as a significant constraint in producing an efficient switch.

The Kinetics of KL Formation Is Strongly Dependent on Linker Length

To directly measure whether the length of J1/13 significantly affects the kinetics of KL formation, a fluorescently labeled RNA (Figure 6A) was studied using smFRET to directly observe conformational transitions between the docked and the undocked conformations of individual surface-immobilized RNAs (Figures 6B–6D). This approach was recently used with the WT *env8*HyCbl riboswitch to define the rates of docking and undocking of the KL interaction in the absence and presence of cobalamin (Holmstrom et al., 2014). The results of that study suggested a model whereby cobalamin binding and formation of the regulatory KL must be faster than the rate at which the 30*S* ribosomal subunit binds to L13 to efficiently regulate gene expression, an effect that is amplified by the physical coupling of transcription and translation in bacteria (Burmann et al., 2010; Proshkin et al., 2010).

The smFRET analysis of cobalamin-independent, Mg^{2+}-dependent KL formation of riboswitches with linker lengths of 7 (WT), 25, and 36 nucleotides revealed the length of J1/13 significantly affects the rate of L5–L13 docking (Figures 6E and 6F). At 5 mM Mg^{2+}, the WT linker promotes ~5-fold faster docking than that of the 36-nucleotide linker. In contrast, the length of J1/13 only weakly affects the rate of undocking of the L5–L13 interaction (Figures 6G and 6H). The diminished rate of docking increases the time that the molecule spends in the undocked conformation without appreciably altering the time spent in the docked conformation. These two effects have the net result of increasing the time-averaged fractional occupancy of the undocked, unrepressed conformation, thereby allowing a higher frequency of translation initiation.

Unfortunately, HyCbl-dependent fluorescence quenching significantly impedes observation of loop docking while ligand is bound to surface-immobilized molecules (Holmstrom et al., 2014). Nevertheless, it is expected that longer linkers would dock less frequently when ligand is bound to the RNA (i.e., slower docking rate constant). As support for such an expectation, free-diffusion smFRET experiments with an enhanced signal-to-noise ratio (but limited observation times) have been used to overcome the effects of HyCbl quenching. As expected, these experiments reveal riboswitches with longer linkers are systematically more undocked regardless of whether ligand is bound (Figures S7A–S7D). These results suggest that in the cell-based activity assay, as the length of J1/13 increases, the decreased rate of interdomain loop-loop docking dictates the loss of efficient repression of reporter expression.

mRNA Abundance Is Controlled by the Rate of KL Formation

For many mRNAs in *E. coli*, a direct consequence of active translation is an increase in their stability due to protection against rho-dependent transcriptional termination or nucleolytic degradation (Boudvillain et al., 2013; Deana and Belasco, 2005). To address this aspect of expression, northern blot analysis of mRNA levels from *E. coli* expressing the WT riboswitch and select linker mutants was performed using cells grown in the presence or absence of HyCbl. For cells grown in the absence of HyCbl, the abundance of mRNA as a function of length increases moderately, in support of increased ribosomal access to the mRNA as the receptor and regulatory domains become further separated (Figures 7A and 7B) and therefore associate less frequently (Figure 6C). In the presence of HyCbl, cells expressing riboswitches with 4-, 14-, and 25-nucleotide linkers showed similarly depressed levels of GFPuv mRNA compared to the WT RNA. In contrast, cells grown in the presence of ligand expressing the mutant riboswitch with a 36-nucleotide linker or the L5(5′-UGAAAG-3′) KL knockout—both of which lack regulatory activity, as monitored by reporter protein expression levels—showed mRNA levels significantly higher than those of the WT riboswitch (Figures 7A and 7C). While these results reveal that mRNA abundance is strongly correlated with cobalamin-dependent regulation, the exact mechanism by which these two observations are linked is unclear.

DISCUSSION

The work presented here is a comprehensive characterization of the sequence and structural elements of a riboswitch regulatory domain and their relationship to ligand-dependent function. The key structural feature directly linking cobalamin binding to translation inhibition is the unpaired nucleotides in the KL interaction that allows this RNA to act as a molecular switch. Specifically, bound cobalamin directly interacts with L5 and L13 to stabilize the docked conformation, which sequesters the RBS, whereas these conserved structural irregularities destabilize this interaction in the absence of cobalamin to allow for translation initiation. While this analysis reveals a functional role for bulged nucleotides within this motif, non-Watson-Crick base pairs have been shown to occur in the KL module of the dimerization site of the HIV-1 RNA, as well as the recently solved structure of the Varkud satellite ribozyme (Paillart et al., 1997; Suslov et al., 2015).

In the presence of bound cobalamin, the frequency of ribosome loading is dependent on the rate of docking between the two loops that form the KL. Previous smFRET experiments using a synthetic RNA designed to mimic the tetraloop-receptor interaction in the P4–P6 domain of the *Tetrahymena* group I intron showed the docking kinetics were relatively tolerant of both the sequence and the length of a single-stranded linker connecting the two domains (Downey et al., 2006). For the cobalamin riboswitch, we demonstrate a similar tolerance for the sequence composition of its linker. However, linker lengths exceeding 25 nucleotides significantly diminish regulatory function, suggesting spatial proximity of the two domains is a critical constraint on gene regulation. Similar effects of proximity and local concentration have been proposed for a range of genetic regulatory systems, including those in bacteria that use the protein Hfq to stabilize duplex formation between small regulatory RNAs and regions that overlap with the RBS of a variety of mRNAs (Vogel and Luisi, 2011). In the case of the cobalamin riboswitch, cobalamin acts analogously to Hfq to promote and stabilize an RNA-RNA interaction, giving rise to more rapid formation of the regulatory KL and limiting the amount of time available for ribosomes to initiate protein synthesis. Furthermore, these strong kinetic constraints on regulation provide an explanation as to why KL assembly for this family of cobalamin riboswitches is observed to occur only as an intramolecular interaction (i.e., in *cis*) rather than through association of the receptor and regulatory SL as independent transcriptional products (i.e., in *trans*). While the potential for ligand-dependent RNA-RNA association in *trans* has been proposed for cobalamin (Peselis and Serganov, 2012) and ZTP (Jones and Ferré-D'Amaré, 2015) riboswitches—both comprising two domains separated by a flexible linker—this mechanism is unlikely to occur in a biological context because of strong temporal constraints placed on the association of these elements and their ability to compete with the gene expression machinery to elicit a regulatory response.

Our results establish that in addition to directly regulating translation initiation through RBS occlusion, ligand binding indirectly modulates mRNA abundance to elicit the full regulatory response. Cobalamin-directed control of mRNA abundance can occur in several ways. In one possible mechanism, translation inhibition resulting from KL stabilization by bound cobalamin allows the RNA-dependent helicase and translocase rho to bind to the nascent RNA and terminate transcription by displacing RNA polymerase. Rho-dependent transcription termination has been implicated in regulating the expression of a variety of mRNAs in *E. coli*, including Mg^{2+}- and flavin mononucleotide-binding riboswitches (Hollands et al., 2012; Peters et al., 2009). Alternatively, expression of many transcripts in both *E. coli* and *B. subtilis* has been shown to be regulated by the interplay between the translational machinery and factors that promote mRNA degradation (Dreyfus, 2009; Yao et al., 2008). In early characterization of the AdoCbl-binding *E. coli btuB* riboswitch that controls translation initiation, it was observed that fusions of the leader region to a *lacZ* reporter exhibited weak ligand-dependent regulation of gene expression. Instead, portions of the *btuB* coding region were required to elicit the full regulatory response, which was interpreted as a region necessary for facilitating mRNA decay (Nou and Kadner, 1998). More recently, degradation of the translationally regulating *E. coli thiM* (thiamine pyrophosphate) riboswitch was shown to be the result of ligand-dependent RBS sequestration that inhibits translation initiation (Caron et al., 2012). This contrasts with

results presented within the same study showing the *E. coli lysC* (lysine) riboswitch controls gene expression through a combination of ligand-dependent RBS occlusion and exposure of specific RNase E sites that can be decoupled. Our results indicate that like the *thiM* and *btuB* riboswitches, translational regulation by the *env8*HyCbl riboswitch is achieved in concert with general mechanisms controlling mRNA stability and abundance. The generality and prevalence of this regulatory scheme suggests that it extends beyond these examples and is applicable to a broad range of riboswitches that modulate the frequency of translation initiation via RBS sequestration. Together, these studies reveal that translational regulation by riboswitches not only is a thermodynamically controlled switch acting upon ribosome loading but also requires factors that modulate mRNA abundance and decay that impart powerful kinetic constraints on their regulatory activity in a cellular context.

EXPERIMENTAL PROCEDURES

RNA Synthesis and Preparation

For all in vitro assays, templates for RNA transcription were synthesized using recursive PCR and transcribed by T7 RNA polymerase using previously described methods (Supplemental Experimental Procedures). All RNA sequences used in this study are given in Table S2.

Cell-Based Reporter Assays

Plasmids bearing a cobalamin riboswitch-regulated reporter gene (GFPuv) were transformed into *E. coli* strain BW25113(ΔbtuR). For all gene expression assays, 5 μl of a saturated overnight culture was added to 5 ml of a rich defined medium (chemically defined salt broth media; Ceres et al., 2013) supplemented with 100 μg/ml ampicillin and 5 μM HyCbl and grown to mid-log phase at 37°C. From each biological replicate, 300 μl of cells were added to wells in a Greiner 96-well half-area microplate, and GFPuv expression was monitored at a 395 nm excitation wavelength and a 510 nm emission wavelength. All data shown are as average fluorescence values normalized to cell density as determined by optical density 600; normalized fluorescence values for each riboswitch variant were background corrected by subtracting cell density-normalized fluorescence from a pBR327 empty vector control. Fold repression was calculated by dividing the average normalized background-corrected fluorescence values for the unrepressed condition (absence of HyCbl) by the average normalized background-corrected fluorescence values for the repressed condition (presence of HyCbl).

EMSAs

Hairpin RNAs corresponding to P13 and L13 of the *env8*HyCbl riboswitch (nucleotides 89–102) were chemically synthesized and 5′ end labeled with ^{32}P using T4 polynucleotide kinase. For each titration, appropriate concentrations of each aptamer were incubated at 4°C for 30 min in buffer (prepared at 25°C) containing 1 mM $MgCl_2$, 10 μM HyCbl, 0.1 mg/ml BSA, 50 mM Tris-HCl (pH 8.0), 10 mM NaCl, 100 mM KCl, 20% glycerol, and 4 μM $tRNA^{Gly}$. Following equilibration of the aptamer with HyCbl, trace amounts of radiolabeled P13 hairpin were added to the reactions and further incubated at 4°C for 1 hr before native gel electrophoresis. Native gel electrophoresis was performed using a 15% acrylamide gel

supplemented with 1 mM $MgCl_2$ and 0.5× TB (45 mM Tris-HCl, 45 mM borate, [pH 8.1]) buffer at 4°C. Gels were imaged using a Typhoon 9400 PhosphoroImager (Molecular Dynamics), and data quantification was performed using the ImageQuant software suite. Data were fit to a standard two-state binding isotherm using Igor (Wavemetrics; Goodrich and Kugel, 2007).

ITC

ITC was performed using approaches and protocols previously described (Supplemental Experimental Procedures).

Structure Probing of RNA

Chemical probing was performed using NMIA modification of the 2′-OH as previously described (Merino et al., 2005; Wilkinson et al., 2006), with slight modifications (Supplemental Experimental Procedures).

Analysis of mRNA Abundance

E. coli BW25113(ΔbtuR) transformed with riboswitch reporter vectors was grown using the same protocol as for the expression assays. Total cellular RNA was extracted using the RNeasy Mini Kit (QIAGEN) and separated by electrophoresis in 1% denaturing agarose gel containing 6.5% formaldehyde and 1X 3-(*N*-morpholino)propanesulfonic acid (pH 6.0 buffer). RNA was transferred to Hybond-N^+ membrane overnight by capillary action in 10X saline sodium citrate buffer (SSC; 1x: 0.15 M NaCl, 0.015 M Na-citrate [pH 7.0]) and crosslinked to membrane using a CL-1000 UV crosslinking oven (254 nm). The ^{32}P-labeled DNA oligonucleotide probes targeting both glyceraldehyde 3-phosphate dehydrogenase (GAPDH) and GFPuv were hybridized to the membrane in a bath containing 6X SSC buffer, 10× Denhardt's solution (10x: 0.2% [w/v] BSA, 0.2% [w/v] Ficoll 400, 0.2% [w/v] polyvinylpyrrolidone), and 0.1% SDS overnight at 42°C. Blots were washed three times at 42°C, and a final wash was performed at 50°C for 20 min. Before hybridization of the second oligonucleotide, blots were stripped by washing the membranes in ~200 ml of boiling 0.1X SSC and 0.1% SDS three times for 5 min. Blots were imaged using a Typhoon 9400 PhosphoroImager, and data quantification was performed using the ImageQuant software suite. The abundance of GFPuv transcript was calculated by dividing the background-corrected counts of GFPuv by the background-corrected counts of GAPDH.

smFRET Experiments

Riboswitch RNAs used for smFRET studies were generated via enzymatic ligation of commercially synthesized custom oligonucleotides using protocols previously described (Supplemental Experimental Procedures). For single-molecule experiments, an imaging buffer (50 mM HEPES, 25 mM KOH, 10 mM NaOH, 100 mM KCl, 2 mM TROLOX, 100 nM PCD and 5 mM PCA, [pH 7.7]) was used with the required concentration of [$MgCl_2$]. For the free-diffusion experiments, the imaging buffer also contained 250 pM FRET-labeled RNA. All single-molecule experiments were performed on a home-built, inverted, confocal epi-fluorescence microscope with a scanning stage, which has been described previously (Fiegland et al., 2012). Excitation of the donor (Cy3) fluorophores was accomplished using a

pulsed green laser (532 nm, 20 MHz, 10 ps pulse width). When required, pulsed interleaved excitation (PIE, PMC1366845) of the Cy5 acceptor fluorophore was accomplished using a red laser (635 nm, 20 MHz, <100 ps pulse width) triggered, with a 25 ns delay, by the green laser. All emitted fluorescence collected by the microscope objective was focused through a confocal pinhole (35 μm) to spatially reject out-of-plane and off-axis fluorescence before being spatially separated by color (donor and acceptor) and polarization (parallel and perpendicular) to direct them to one of four avalanche photodiodes (PerkinElmer), where the arrival times at each photon are recorded by a time-correlated single-photon counting module (Becker and Hickl). Additional details of surface-immobilized and free-diffusion experiments are provided in Supplemental Experimental Procedures.

Supplementary Material

Refer to Web version on PubMed Central for supplementary material.

Acknowledgments

This work has been funded by a grant from the NIH (R01 GM073850) to R.T.B. and through an award by the NIH/University of Colorado, Boulder Molecular Biophysics Training Program (T32 GM06103) to J.T.P. E.D.H. and D.J.N. gratefully acknowledge support for this work from the National Science Foundation (CHE 1266416 and PHY 1125844) and the National Institute for Standards and Technology.

References

Barrick JE, Breaker RR. The distributions, mechanisms, and structures of metabolite-binding riboswitches. Genome Biol. 2007; 8:R239. [PubMed: 17997835]

Boudvillain M, Figueroa-Bossi N, Bossi L. Terminator still moving forward: expanding roles for Rho factor. Curr Opin Microbiol. 2013; 16:118–124. [PubMed: 23347833]

Burmann BM, Schweimer K, Luo X, Wahl MC, Stitt BL, Gottesman ME, Rösch P. A NusE:NusG complex links transcription and translation. Science. 2010; 328:501–504. [PubMed: 20413501]

Butcher SE, Pyle AM. The molecular interactions that stabilize RNA tertiary structure: RNA motifs, patterns, and networks. Acc Chem Res. 2011; 44:1302–1311. [PubMed: 21899297]

Caron MP, Bastet L, Lussier A, Simoneau-Roy M, Massé E, Lafontaine DA. Dual-acting riboswitch control of translation initiation and mRNA decay. Proc Natl Acad Sci USA. 2012; 109:E3444–E3453. [PubMed: 23169642]

Ceres P, Garst AD, Marcano-Velázquez JG, Batey RT. Modularity of select riboswitch expression platforms enables facile engineering of novel genetic regulatory devices. ACS Synth Biol. 2013; 2:463–472. [PubMed: 23654267]

Deana A, Belasco JG. Lost in translation: the influence of ribosomes on bacterial mRNA decay. Genes Dev. 2005; 19:2526–2533. [PubMed: 16264189]

Downey CD, Fiore JL, Stoddard CD, Hodak JH, Nesbitt DJ, Pardi A. Metal ion dependence, thermodynamics, and kinetics for intramolecular docking of a GAAA tetraloop and receptor connected by a flexible linker. Biochemistry. 2006; 45:3664–3673. [PubMed: 16533049]

Dreyfus M. Killer and protective ribosomes. Prog Mol Biol Transl Sci. 2009; 85:423–466. [PubMed: 19215779]

Fiegland LR, Garst AD, Batey RT, Nesbitt DJ. Single-molecule studies of the lysine riboswitch reveal effector-dependent conformational dynamics of the aptamer domain. Biochemistry. 2012; 51:9223–9233. [PubMed: 23067368]

Gao A, Serganov A. Structural insights into recognition of c-di-AMP by the ydaO riboswitch. Nat Chem Biol. 2014; 10:787–792. [PubMed: 25086507]

Goodrich, JA.; Kugel, JF. Binding and kinetics for molecular biologists. CSHL Press; 2007.

Hollands K, Proshkin S, Sklyarova S, Epshtein V, Mironov A, Nudler E, Groisman EA. Riboswitch control of Rho-dependent transcription termination. Proc Natl Acad Sci USA. 2012; 109:5376–5381. [PubMed: 22431636]

Holmstrom ED, Polaski JT, Batey RT, Nesbitt DJ. Single-molecule conformational dynamics of a biologically functional hydroxocobalamin riboswitch. J Am Chem Soc. 2014; 136:16832–16843. [PubMed: 25325398]

Johnson JE Jr, Reyes FE, Polaski JT, Batey RT. B12 cofactors directly stabilize an mRNA regulatory switch. Nature. 2012; 492:133–137. [PubMed: 23064232]

Jones CP, Ferré-D'Amaré AR. Crystal structure of a c-di-AMP riboswitch reveals an internally pseudo-dimeric RNA. EMBO J. 2014; 33:2692–2703. [PubMed: 25271255]

Jones CP, Ferré-D'Amaré AR. Recognition of the bacterial alarmone ZMP through long-distance association of two RNA subdomains. Nat Struct Mol Biol. 2015; 22:679–685. [PubMed: 26280533]

Liberman JA, Suddala KC, Aytenfisu A, Chan D, Belashov IA, Salim M, Mathews DH, Spitale RC, Walter NG, Wedekind JE. Structural analysis of a class III preQ1 riboswitch reveals an aptamer distant from a ribosome-binding site regulated by fast dynamics. Proc Natl Acad Sci USA. 2015; 112:E3485–E3494. [PubMed: 26106162]

McKinney SA, Joo C, Ha T. Analysis of single-molecule FRET trajectories using hidden Markov modeling. Biophys J. 2006; 91:1941–1951. [PubMed: 16766620]

Merino EJ, Wilkinson KA, Coughlan JL, Weeks KM. RNA structure analysis at single nucleotide resolution by selective 2′-hydroxyl acylation and primer extension (SHAPE). J Am Chem Soc. 2005; 127:4223–4231. [PubMed: 15783204]

Nahvi A, Sudarsan N, Ebert MS, Zou X, Brown KL, Breaker RR. Genetic control by a metabolite binding mRNA. Chem Biol. 2002; 9:1043. [PubMed: 12323379]

Nou X, Kadner RJ. Coupled changes in translation and transcription during cobalamin-dependent regulation of btuB expression in *Escherichia coli*. J Bacteriol. 1998; 180:6719–6728. [PubMed: 9852020]

Paillart JC, Westhof E, Ehresmann C, Ehresmann B, Marquet R. Non-canonical interactions in a kissing loop complex: the dimerization initiation site of HIV-1 genomic RNA. J Mol Biol. 1997; 270:36–49. [PubMed: 9231899]

Peselis A, Serganov A. Structural insights into ligand binding and gene expression control by an adenosylcobalamin riboswitch. Nat Struct Mol Biol. 2012; 19:1182–1184. [PubMed: 23064646]

Peters JM, Mooney RA, Kuan PF, Rowland JL, Keles S, Landick R. Rho directs widespread termination of intragenic and stable RNA transcription. Proc Natl Acad Sci USA. 2009; 106:15406–15411. [PubMed: 19706412]

Porter EB, Marcano-Velázquez JG, Batey RT. The purine riboswitch as a model system for exploring RNA biology and chemistry. Biochim Biophys Acta. 2014; 1839:919–930. [PubMed: 24590258]

Proshkin S, Rahmouni AR, Mironov A, Nudler E. Cooperation between translating ribosomes and RNA polymerase in transcription elongation. Science. 2010; 328:504–508. [PubMed: 20413502]

Ren A, Patel DJ. c-di-AMP binds the ydaO riboswitch in two pseudo-symmetry-related pockets. Nat Chem Biol. 2014; 10:780–786. [PubMed: 25086509]

Ren A, Rajashankar KR, Patel DJ. Global RNA fold and molecular recognition for a pfl riboswitch bound to ZMP, a master regulator of one-carbon metabolism. Structure. 2015; 23:1375–1381. [PubMed: 26118534]

Roth A, Breaker RR. The structural and functional diversity of metabolite-binding riboswitches. Annu Rev Biochem. 2009; 78:305–334. [PubMed: 19298181]

Seol Y, Skinner GM, Visscher K, Buhot A, Halperin A. Stretching of homopolymeric RNA reveals single-stranded helices and base-stacking. Phys Rev Lett. 2007; 98:158103. [PubMed: 17501388]

Storz G, Vogel J, Wassarman KM. Regulation by small RNAs in bacteria: expanding frontiers. Mol Cell. 2011; 43:880–891. [PubMed: 21925377]

Suslov NB, DasGupta S, Huang H, Fuller JR, Lilley DM, Rice PA, Piccirilli JA. Crystal structure of the Varkud satellite ribozyme. Nat Chem Biol. 2015; 11:840–846. [PubMed: 26414446]

Trausch JJ, Xu Z, Edwards AL, Reyes FE, Ross PE, Knight R, Batey RT. Structural basis for diversity in the SAM clan of riboswitches. Proc Natl Acad Sci USA. 2014; 111:6624–6629. [PubMed: 24753586]

Trausch JJ, Marcano-Velázquez JG, Matyjasik MM, Batey RT. Metal ion-mediated nucleobase recognition by the ZTP riboswitch. Chem Biol. 2015; 22:829–837. [PubMed: 26144884]

Vitreschak AG, Rodionov DA, Mironov AA, Gelfand MS. Regulation of the vitamin B12 metabolism and transport in bacteria by a conserved RNA structural element. RNA. 2003; 9:1084–1097. [PubMed: 12923257]

Vogel J, Luisi BF. Hfq and its constellation of RNA. Nat Rev Microbiol. 2011; 9:578–589. [PubMed: 21760622]

Wilkinson KA, Merino EJ, Weeks KM. Selective 2′-hydroxyl acylation analyzed by primer extension (SHAPE): quantitative RNA structure analysis at single nucleotide resolution. Nat Protoc. 2006; 1:1610–1616. [PubMed: 17406453]

Yao S, Blaustein JB, Bechhofer DH. Erythromycin-induced ribosome stalling and RNase J1-mediated mRNA processing in *Bacillus subtilis*. Mol Microbiol. 2008; 69:1439–1449. [PubMed: 18647167]

Highlights

- Structural features needed for a cobalamin-dependent regulatory switch are identified
- Spatial relationship between receptor and regulatory domains is critical for function
- Translation initiation is controlled by the kinetics of the interdomain interaction
- Efficient regulation by a translational riboswitch involves other cellular factors

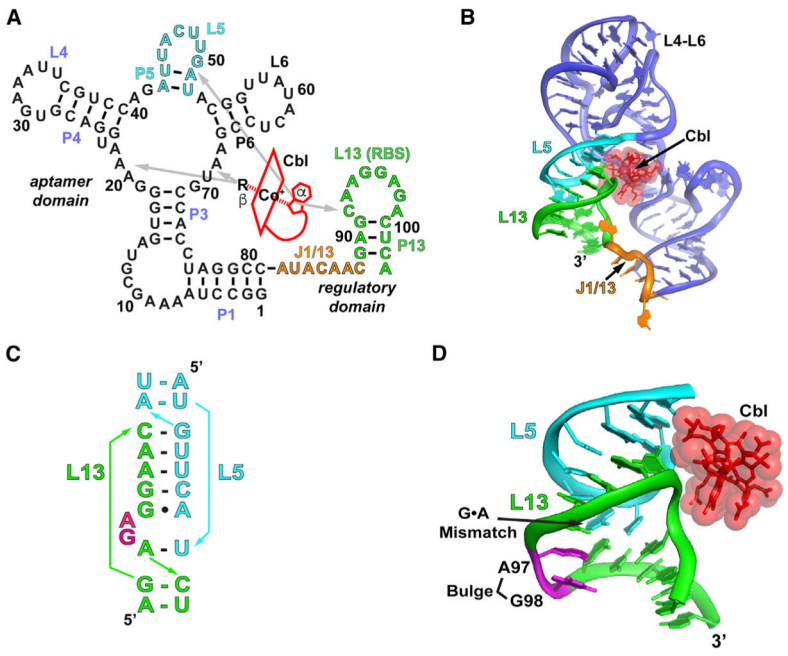

Figure 1. Secondary and Tertiary Structure Schematic of the *env8*HyCbl Riboswitch

(A) Sequence and secondary structure of the WT *env8*HyCbl riboswitch. L13 within the regulatory domain contains the RBS. A schematic representation of cobalamin is shown in red, with contacts between cobalamin and the RNA depicted by gray arrows.

(B) Tertiary structure of the WT riboswitch with the regulatory KL formed by the interaction between L5 and L13 highlighted in cyan and green, respectively. Bound cobalamin is shown in red, and the single-stranded linker connecting P1 and P13 (J1/13) is highlighted in orange.

(C) Sequence and secondary structure of the KL interaction in the presence of bound cobalamin. Coloring corresponds to (B), with the exception of two conserved unpaired nucleotides (A97 and G98) highlighted in magenta.

(D) Close up of the KL interaction, emphasizing its direct contacts with cobalamin and the positioning of the unpaired nucleotides A97 and G98.

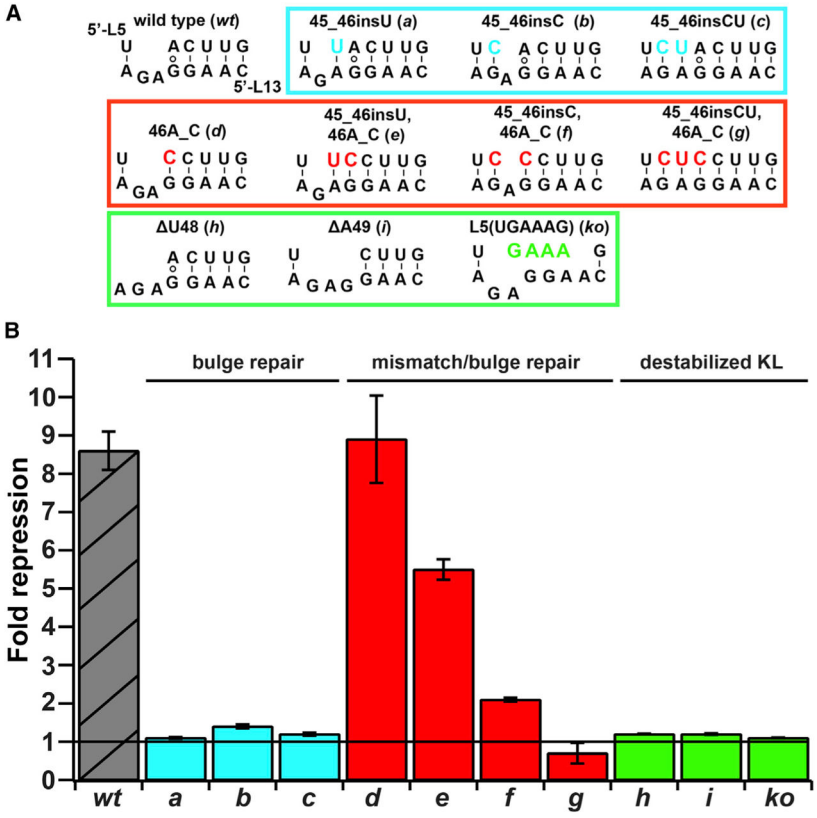

Figure 2. Regulatory Activity Is Dependent on the Presence of Unpaired Nucleotides in the L5–L13 KL Interaction

(A) KL sequences of the WT riboswitch and constructs carrying mutations in L5. Mutations made to L5 are highlighted using colors that correspond to the boxes, which group them according to type. Sequences boxed in cyan carry insertions in the presence of the A•G purine-purine base pair (bulge repair). Sequences boxed in red feature a Watson-Crick C–G base pair in place of the A•G purine-purine pair, as well as insertions in the presence of the C–G pair (mismatch or bulge repair). Sequences boxed in green carry deletions or a 5′-GAAA-3′ tetraloop mutation in L5 that destabilizes the KL interaction (destabilized KL).

(B) Fold repression values for the WT riboswitch (striped gray bar) and riboswitch mutants shown in (A) are depicted as the ratio of fluorescence from cells grown in the absence of HyCbl to cells grown in the presence of HyCbl. The colors of the bars correspond to the colors of the boxed sequences in (A).

Data are represented as mean ± SEM of triplicate measurements from at least three biological replicates.

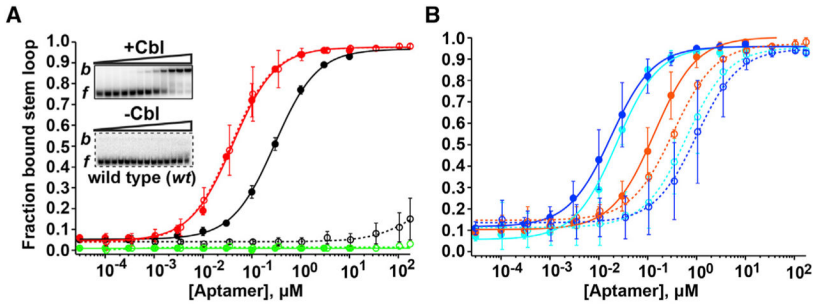

C

Riboswitch	+Cbl	K_D (nM)	-Cbl	K_D (nM)	K_{rel} ($K_{D(-HyCbl)}/K_{D(+HyCbl)}$)
wild type (*wt*)	●	290 ± 9	⊖	> 2000000	> 6,800
45_46insCU, 46A_C (*g*)	●	41 ± 3	⊖	38 ± 1	0.93
L5(UGAAAG) (*ko*)	●	N.D.	⊖	N.D.	N.D.
46A_C (*d*)	●	23 ± 3	⊖	620 ± 24	27
45_46insC, 46A_C (*f*)	●	18 ± 1	⊖	1000 ± 48	56
45_46insU, 46A_C (*e*)	●	140 ± 7	⊖	340 ± 16	2.4

Figure 3. Cobalamin-Dependent Differences in Affinity between Receptor and Regulatory Domains in *trans* Highlight the Complex Requirements of Gene Regulation In Vivo

(A) Quantified gel shift data performed in the presence of HyCbl for the WT (ΔJ1/13, ΔP13) receptor domain (*wt*, filled black circles and solid black line), the 45_46insCU, 46A_C mutant (*g*, filled red circles and solid red line), and the L5(5′-UGAAAG-3′) mutant (*ko*, filled green circles and green line). Quantified EMSA data for these same sequences conducted in the absence of cobalamin are shown using corresponding colors with open circles and dashed lines. Representative gel shifts performed in the presence and absence of cobalamin using the WT aptamer are shown as insets, where *b* represents bound SL13 and *f* represents free SL13. Data are represented as mean ± SD of three titrations for each construct.

(B) Quantified gel shifts performed in the presence of HyCbl for the 46A_C mutant aptamer (*d*, filled cyan circles and solid cyan line), the 45_46insU, 46A_C mutant (*e*, filled orange circles and solid orange line), and the 45_46insC, 46A_C mutant (*f*, filled blue circles and solid blue line). Quantified EMSA data for these same sequences conducted in the absence of cobalamin are shown using corresponding colors with open circles and dashed lines. Data are represented as mean ± SD of three titrations for each construct.

(C) Legend and dissociation constants for each of the curves depicted in (A) and (B).

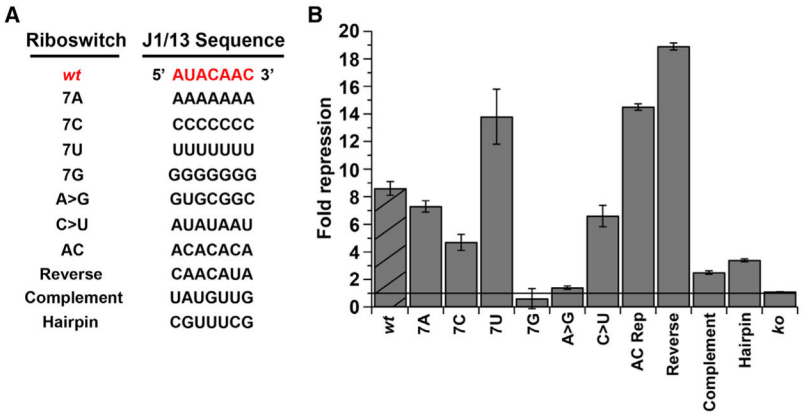

Figure 4. Regulatory Activity Is Tolerant of Sequence Alterations to J1/13

(A) Mutations made to the linker sequence (J1/13). The WT linker sequence is shown at the top and is colored red.

(B) Fold repression data from the GFPuv reporter assay for cells expressing the WT riboswitch (striped bar) and mutant riboswitches shown in (A) were calculated in the same manner as in Figure 2B. Data are represented as mean ± SEM of triplicate measurements from at least three biological replicates.

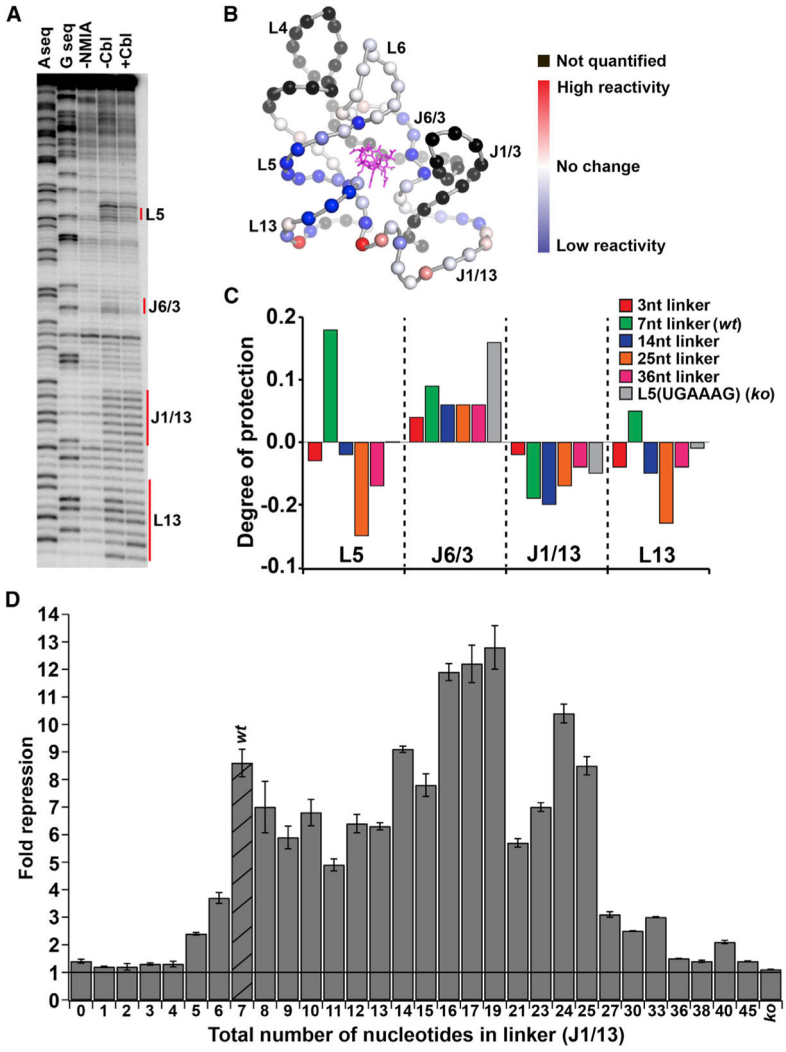

Figure 5. Regulatory Activity Varies as a Function of the Distance Separating the Receptor Domain and Expression Platform

(A) Representative SHAPE gel of the WT riboswitch probed in the absence and presence of HyCbl (two right lanes). The two left lanes are A and G sequencing reactions, and the "-NMIA" lane indicates background signal. Regions of interest in the gel are denoted with a red bar.

(B) SHAPE reactivity profile from the gel shown in (A) projected onto the crystal structure of the WT riboswitch. Black spheres represent nucleotides that were not quantified, blue spheres represent bases that show decreased reactivity in the presence of ligand, red spheres represent bases that show increased reactivity in the presence of ligand, and white spheres represent bases that show no change in reactivity in the presence of ligand.

(C) Quantified SHAPE reactivity profiles of a subset of mutants with varying linker lengths. Quantified data are grouped by regions of interest for each construct and correspond to the vertical red bars in (A). Negative values indicate a higher degree of reactivity with NMIA in the presence of ligand, and positive values indicate a lower degree of NMIA reactivity in the presence of ligand.

(D) Fold repression values for cells expressing the WT riboswitch (striped bar) and linker length variants as reported by expression of GFPuv. The construct labeled *ko* at the far right is the L5(5′-UGAAAG-3′) mutant that is unable to form the regulatory KL. Longer lengths of J1/13 were made by addition of nucleotides to the 3′ end of the WT linker, while shorter linkers were created by deletion from the 3′ end. Nucleotide addition to the 3′ end of J1/13 followed a repetitive pattern of the WT sequence.

Data are represented as mean ± SEM of triplicate measurements from at least three biological replicates.

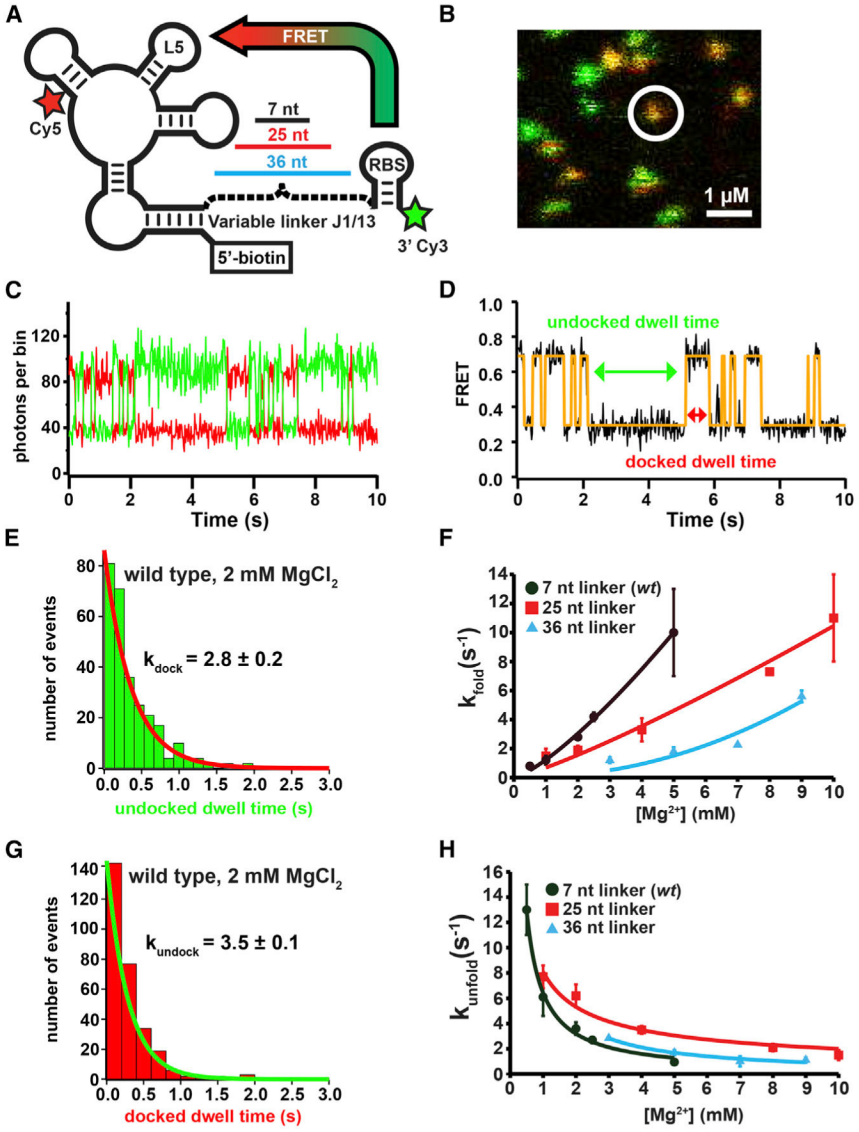

Figure 6. Length of Linker J1/13 Influences the Rate of Association of L5 and L13

(A) Cartoon representation of the secondary structure and synthetic modifications associated with the RNAs used for smFRET. A Cy3 donor (green star) was appended to the 3′ terminus of the RNA, a Cy5 acceptor (red star) was incorporated at position U24 in P4, and biotin was attached at the 5′ end for immobilization to a glass coverslip.

(B) Representative image of a red-green, false-color, FRET-efficiency surface scan generated by rastering an area of the coverslip through the focus of the microscope objective.

(C) Anti-correlated fluctuations in donor and acceptor fluorescence of the WT RNA correspond to transitions between the docked conformations (high E_{FRET}) and the undocked conformations (low E_{FRET}) of the KL (2 mM $MgCl_2$).

(D) Corresponding FRET-efficiency trajectory (black) of the WT riboswitch and a two-state hidden-Markov model (orange; McKinney et al., 2006).

(E) Histograms of the undocked dwell times used to determine the docking rate constants.

(F) Docking rate constants representing KL formation in the absence of HyCbl as a function of Mg^{2+} concentration for the WT riboswitch (black circles and line) and mutants with 25-nucleotide linkers (red squares and line) and 36-nucleotide linkers (cyan triangles and line).
(G) Histograms of the docked dwell times used to determine the undocking rate constants.
(H) Undocking rate constants representing KL undocking in the absence of HyCbl as a function of Mg^{2+} concentration for the WT riboswitch (black circles and line) and mutants with 25-nucleotide linkers (red squares and line) and 36-nucleotide linkers (cyan triangles and line).
Solid lines are not intended to represent fits of the various datasets and serve only as a visual guide to demonstrate the observed trends.

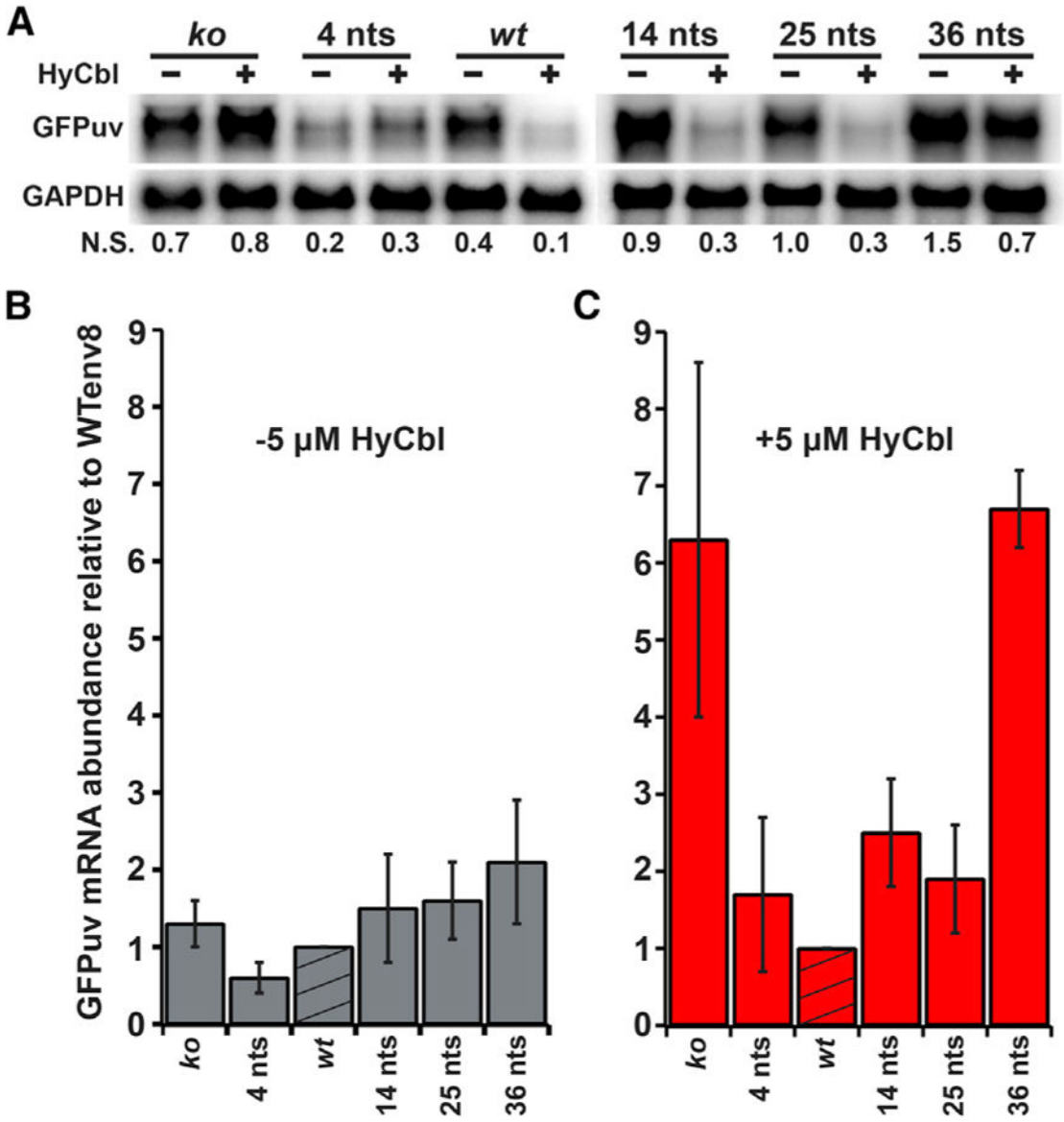

Figure 7. Translational Repression by Cobalamin Influences Transcript Abundance

(A) Representative gel showing northern blot detection of GFPuv and GAPDH mRNAs in cells grown in the absence and presence of HyCbl expressing the WT riboswitch, the L5(5′-UGAAAG-3′) mutant, and constructs with 4-, 14-, 25-, and 36-nucleotide linkers. Numbers denoting the normalized signal (N.S.) below each lane represent the ratio of GFPuv counts to GAPDH counts.

(B) Bar graph representation of GFPuv mRNA abundance in cells expressing each mutant riboswitch relative to GFPuv mRNA abundance in cells expressing the WT RNA (striped bar) grown in the absence of HyCbl.

(C) Bar graph representation of GFPuv mRNA abundance in cells expressing each mutant riboswitch relative to GFPuv mRNA abundance in cells expressing the WT RNA (striped bar) grown in the presence of HyCbl.

Data are represented as mean ± SD of three biological replicates for each construct.